Microporous and Mesoporous Materials 185 (2014) 149–156

Contents lists available at ScienceDirect

Microporous and Mesoporous Materials

journal homepage: www.elsevier.com/locate/micromeso

Synthesis of ZSM-2 nanocrystals at ambient temperature

Danhua Yuan [a,b,c], Shutao Xu [a,b], Mozhi Zhang [a,b,c], Yingxu Wei [a,b], Xinglong Dong [a,b,c], Yanli He [a,b], Shuliang Xu [a,b], Zhongmin Liu [a,b,*], Yunpeng Xu [a,b,*]

[a] National Engineering Laboratory for Methanol to Olefins, Dalian Institute of Chemical Physics, Chinese Academy of Sciences, P. O. Box 110, 116023 Dalian, PR China
[b] Dalian National Laboratory for Clean Energy, Dalian Institute of Chemical Physics, Chinese Academy of Sciences, Dalian, PR China
[c] Graduate University of Chinese Academy of Sciences, Beijing 100049, PR China

ARTICLE INFO

Article history:
Received 22 September 2013
Received in revised form 25 October 2013
Accepted 4 November 2013
Available online 13 November 2013

Keywords:
ZSM-2
Ambient temperature
Synthesis
Crystallization process

ABSTRACT

ZSM-2 nanorods with crystal size around 50 nm were successfully synthesized at ambient temperature (30 °C). The crystallization process of ZSM-2 zeolite under ambient temperature was studied and discussed according to the measurement of crystallization kinetic curve, and characterizations with multiple techniques, such as X-ray diffraction (XRD), scanning electron microscopy (SEM), low-temperature N_2 adsorption/desorption analysis, thermogravimetry analysis (TG) and nuclear magnetic resonance (NMR) etc. The ZSM-2 zeolite synthesized at ambient temperature presented different crystal morphologies and large specific area as compared with the sample synthesized at high temperature (100 °C). Furthermore, ^{29}Si MAS-NMR showed that the nanoscale ZSM-2 obtained by ambient synthesis contained more EMT phase and lower Si/Al ratio than that of micrometer-sized ZSM-2 crystals obtained at 100 °C. More interestingly, NMR and low-temperature N_2 adsorption/desorption characterizations revealed that the local environment of Al did not change much while that of Si did change a lot during the ambient crystallization process, and the micropore area increased rapidly while the micropore size distributions of the samples changed little with increasing crystallization time.

1. Introduction

Zeolite ZSM-2 possesses the super-cage structure with 12-ring opening pores, and has been described as an intergrowth of cubic FAU structure (faujasite) and hexagonal EMT structure (hexagonal faujasite) [1]. The ZSM-2 zeolite, due to its similar acidity and structure as the most important catalyst of zeolite Y (FAU), has great potential in its applications in the fluidized-bed catalytic cracking (FCC) process as a candidate catalyst [2]. ZSM-2 zeolite was originally synthesized by aging aqueous solution of amorphous glasses (Li_2O–Al_2O_3–SiO_2) at room temperature, followed by hydrothermal treatment at 55–60 °C for 30 days and in this way, ZSM-2 zeolite crystals sized approximately in 0.5 μm could be obtained [3]. Subsequently, Barrer and Sieber [4] obtained the platelet ZSM-2 zeolite crystals with diameter about 0.75–1.0 μm from the gels prepared by adding the solution of lithium and cesium to tetramethylammonium (TMA)-aluminosilicate solution, and the crystallization temperature was 90 °C. After that, Schoeman et al. [5] synthesized ZSM-2 with crystal sizes less than 100 nm by heating the gels of TMA-aluminosilicate solution together with lithium cation at 100 °C for 12 h.

Nanosized zeolites exhibit distinct advantages over conventional micrometer-sized zeolites in catalytic and sorption processes due to their larger external surface areas, higher surface activity and lower mass and heat transfer resistance [6]. Zeolite nanocrystals could be obtained via clear solutions synthesis [7–11], confined-space synthesis [12–14], or ambient synthesis etc. [15–17]. Among these synthesis strategies, the ambient synthesis opened new avenues for fundamental studies of zeolite nucleation and growth processes due to its slow crystal growth kinetics, in addition to its economic and environmental benefits [16,17]. For instance, Mintova successfully synthesized LTA-type crystals at room temperature and predicted that the LTA-type zeolite crystallization process was mainly a solution-mediated mechanism [10]. Sand et al. obtained zeolite A with a crystallinity of about 75% from a conventional template free Na_2O–Al_2O_3–SiO_2–H_2O system after 28 days at room temperature [15]. The template free synthesis of FAU-type zeolite at room temperature was reported and zeolite nucleation and crystallization process was studied by TEM [16]. Very recently, ultrasmall hexagonal EMT nanocrystals had been synthesized at ambient temperature of 30 °C without using any organic template [17]. In brief, the ambient synthesis conditions restricted the growth of zeolite crystals and facilitated the generation of nanocrystals. Especially the slow crystal growth kinetics at room

* Corresponding authors at: National Engineering Laboratory for Methanol to Olefins, Dalian Institute of Chemical Physics, Chinese Academy of Sciences, P. O. Box 110, 116023 Dalian, PR China. Tel./fax: +86 0411 84379518.
E-mail addresses: liuzm@dicp.ac.cn (Z. Liu), xuyp@dicp.ac.cn (Y. Xu).

1387-1811/$ - see front matter © 2013 Elsevier Inc. All rights reserved.
http://dx.doi.org/10.1016/j.micromeso.2013.11.010

temperature allowed us to study the crystallization process of zeolite.

In this study we have successfully synthesized ZSM-2 nanocrystals at ambient temperature of 30 °C. The crystallization process of ZSM-2 nanocrystals was studied by X-ray diffraction (XRD), scanning electron microscopy (SEM), low-temperature N_2 adsorption/desorption analysis, thermogravimetry analysis (TG) and nuclear magnetic resonance (NMR) etc. The effects of crystallization time on the ambient synthesis were investigated, and the characteristics of nanosized ZSM-2 zeolite obtained by ambient synthesis were compared with those of micrometer-sized ZSM-2 zeolite crystallized at high temperature (100 °C). Furthermore, we investigated the transformation of the Al and Si coordination state and textural properties during the ambient crystallization process by means of MAS-NMR and low-temperature N_2 adsorption/desorption characterizations.

2. Experimental section

2.1. Synthesis

The chemical reagents used in the experiments included tetraethyl orthosilicate (TEOS, ⩾98%, Tianjin Kemiou Chemical Reagent Co. Ltd.,), aluminium isopropoxide (AIP, Al_2O_3 ⩾ 24.7 wt%, Sinopharm Chemical Reagent Co. Ltd.,), LiOH (⩾98%, Aladdin Chemistry Co. Ltd.,), tetramethylammonium hydroxide (TMAOH, 25% in water, Aladdin Chemistry Co. Ltd.,). All the above reagents were used without further purification.

A typical synthesis procedure was as follows. Firstly, organic amine, AIP, and water were added into a plastic beaker with stirring at room temperature to prepare a clear aluminate solution. Next, appropriate amount of TEOS was directly mixed with the freshly prepared aluminate solution under stirring for 2 h so as to obtain a clear aluminosilicate solution. Then, the LiOH solution was dropwise added into the above obtained aluminosilicate solution with strong agitation to get the final gel with molar composition of 2.5LiOH:1AIP:2.5TEOS:2.5TMAOH:435H_2O. This mixture was aged for 4 h with agitation and then transferred into a stainless steel autoclave, placed in an oven statically at the ambient temperature (30 °C) or high temperature (100 °C) for a certain time. After the crystallization, the powdered products were recovered with centrifugation, washed with deionized water until pH < 8, and then dried at room temperature for 24 h for further characterization. The sample synthesized at 100 °C for 2.5 days was named as sample HS. The samples crystallized at 30 °C for 0, 3, 4, 4.5, 5, 5.5, 6, 7, 9, 15, 18, 24, and 27 days were named as 0 d, 3 d, 4 d, 4.5 d, 5 d, 5.5 d, 6 d, 7 d, 9 d, 15 d (AS), 18 d, 24 d, and 27 d, respectively. The ambient crystallization kinetic curve of ZSM-2 zeolite was plotted against the relative crystallinity which was evaluated according to the first peak intensities of the XRD patterns. The sample of 15 d with the first peak intensity reaching the maximum was defined as completely (100%) crystalline. Calcination was carried out at 400 °C for 2 h to remove organic species.

2.2. Characterization

As-synthesized products were examined using X-ray powder diffraction (XRD) for phase identification. The X-ray diffraction patterns were recorded with a PANalytical X'Pert PRO X-ray diffractometer using the Cu-Kα radiation (λ = 1.54059 Å), operating at 40 kV and 40 mA. The crystal size and morphology were measured by a Hitachi SU8020 scanning electron microscopy. All the solid state NMR experiments were performed on a Bruker AvanceIII 600 spectrometer equipped with a 14.1 T wide-bore magnet. The resonance frequencies were 156.4 and 119.2 MHz for ^{27}Al and ^{29}Si, respectively. ^{27}Al MAS-NMR experiments were performed on a 4 mm MAS probe with a spinning rate of 13 kHz. ^{27}Al MAS-NMR spectra were recorded using one pulse sequence. 600 scans were accumulated with a $\pi/8$ pulse width of 0.75 μs and a 2 s recycle delay. Chemical shifts were referenced to (NH_4)-$Al(SO_4)_2 \cdot 12H_2O$ at −0.4 ppm. ^{29}Si MAS-NMR spectra were recorded with a 7 mm MAS probe with a spinning rate of 5 kHz using high-power proton decoupling. 1024 scans were accumulated with a $\pi/4$ pulse width of 2.5 μs and a 10 s recycle delay. Chemical shifts were referenced to 4,4-dimethyl-4-silapentane sulfonate sodium salt (DSS). Textural properties of the calcined samples were determined by N_2 adsorption–desorption isotherms at 77 K on a Micromeritics ASAP 2020 system. The total surface area was calculated based on the BET equation. The micropore volume and micropore surface area were evaluated using the *t*-plot method. The micropore size and mesopore size distributions were calculated using the HK method and BJH method, respectively. The thermogravimetry analysis was performed using a TA Q-600 analyzer. The samples were heated from room temperature to 900 °C with a heating rate of 10 °C/min in an air flow of 100 ml/min. The contents of water and template in the as-synthesized samples were calculated according to the weight losses at the temperature lower

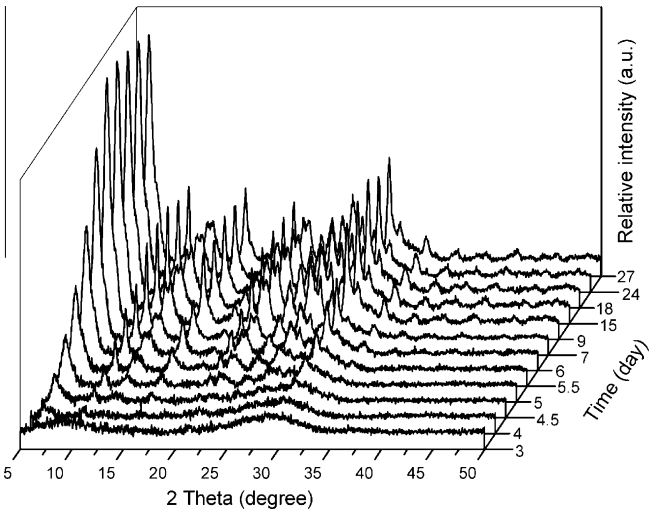

Fig. 1. XRD patterns of the samples corresponding to ambient crystallization curve.

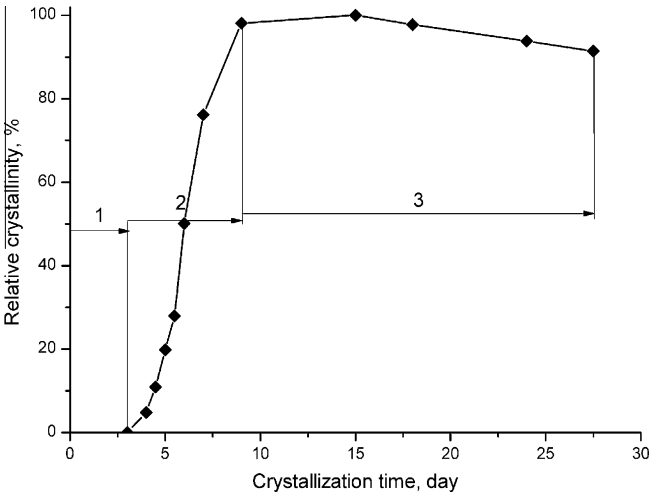

Fig. 2. Ambient crystallization kinetic curve of nanoscale ZSM-2 crystals.

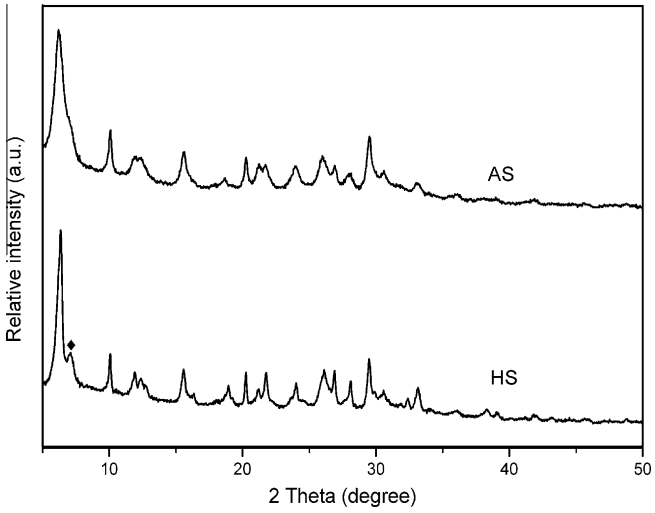

Fig. 3. XRD patterns of as-synthesized sample HS and sample AS. (♦ the peak at 2θ of about 7.15°).

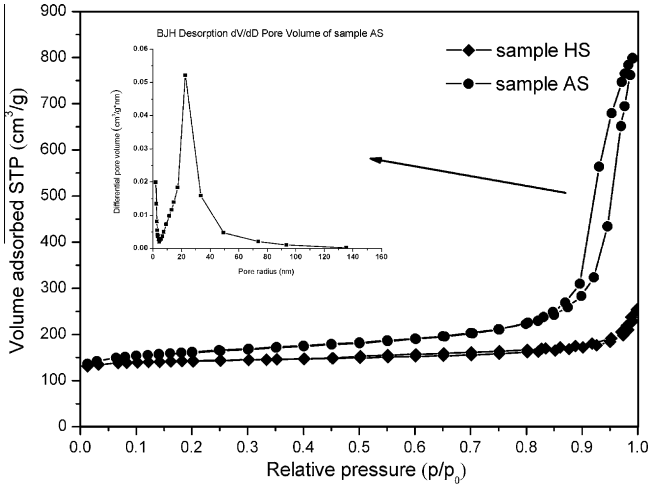

Fig. 5. N_2 adsorption–desorption isotherms of as-synthesized sample HS and sample AS.

than 300 °C and in the range of 300–600 °C in the TG curve, respectively.

3. Results and discussion

3.1. Ambient synthesis of ZSM-2 nanocrystals

The XRD patterns of the samples corresponding to the crystallization time are shown in Fig. 1 and the ambient crystallization kinetic curve of ZSM-2 nanocrystals (Fig. 2) was plotted according to the relative crystallinity of the samples shown in Fig. 1. As shown in Fig. 2, the ambient crystallization kinetic curve exhibited typical three stages [18,19]. First stage with no apparent diffraction peak in the XRD patterns from 0 day to 3 days could be defined as inducing period, which comprised the dissolution of the raw material and the process of spontaneous nucleation [18]. Then the second stage up to 9 days with the crystallinity linearly increasing to 98% was identified as the period for continuous growth on the spontaneous nuclei produced in the first stage. In this process, the XRD patterns showed the peaks corresponding to ZSM-2 zeolite, and the intensities of the peaks linearly increased with increasing hydrothermal crystallization time. The crystallization process was completed at 15 days with the crystallinity up to 100%. This stage with the crystallinity maintaining at more than 90% from 9 days to 27 days, was belonged to the period of re-crystallization and perfection of the zeolite crystallites.

3.2. Comparison of ZSM-2 crystallized at high temperature (100 °C) and ambient temperature (30 °C)

The temperature was of great importance for the zeolite crystallization. The properties of ZSM-2 zeolite synthesized at high temperature of 100 °C for 2.5 days (sample HS) and at ambient

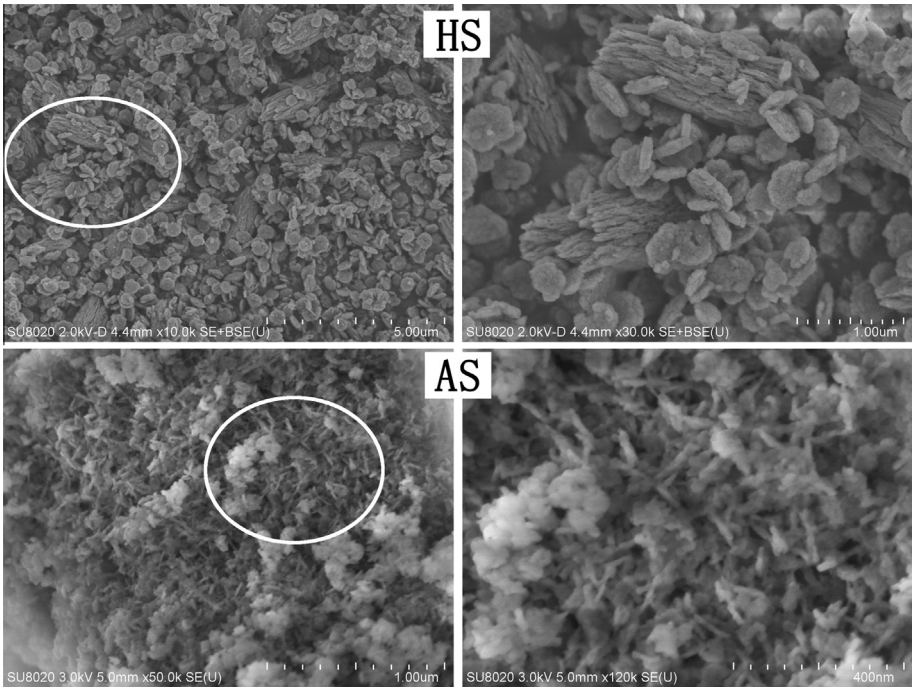

Fig. 4. SEM images of as-synthesized sample HS and sample AS.

Table 1
Textual properties of sample HS and sample AS.

Sample	Surface area (m^2/g)			Pore volume (cm^3/g)	
	S_{total}[a]	S_{micro}[b]	S_{ext}[c]	V_{total}	V_{micro}[d]
HS	425	364	61	0.27	0.17
AS	550	359	190	1.00	0.17

[a] BET surface area.
[b] *t*-plot micropore surface area.
[c] *t*-plot external surface area.
[d] *t*-plot micropore volume.

Table 2
Thermogravimetry analysis results of sample HS and sample AS.

Sample	Weight loss (%)		
	I (<300 °C)	II (300–600 °C)	III (600–900 °C)
HS	17.91	3.85	0.16
AS	20.66	8.53	0.48

temperature of 30 °C for 15 days (sample AS) were compared in this section. The XRD patterns of sample HS and sample AS shown in Fig. 3 exhibited the similar crystallinity. Since the slow kinetic process, the ambient synthesis required longer time to obtain the same crystallinity of ZSM-2 zeolite as that synthesized at 100 °C. Both of sample HS and sample AS exhibited typical X-ray reflection peaks of ZSM-2 zeolite without any detectable impurities. However, there was still some slight difference observed in the X-ray diffraction patterns of sample HS and sample AS. In particular, the peak observed at 2θ of about 7.15° in the XRD pattern of sample HS almost disappeared in the XRD pattern of sample AS. The diffraction peaks of sample AS significantly broadened as compared with those of sample HS, which could be attributed to the small zeolite crystal size [20,21]. As shown in Fig. 4, the crystal size of sample HS was about 1–2 μm and that of sample AS was 50 nm in length. Sample HS and sample AS also displayed very different morphologies as shown in Fig. 4. Sample HS appeared with two different morphologies, one was plate-like crystal with size of about 0.5 μm, and another was the aggregation of rods with crystal size of about 1–2 μm. But the sample AS was mainly composed of rod-like particles of ZSM-2 with crystal sizes around 50 nm in length.

The textural properties of sample HS and sample AS were characterized by nitrogen physical adsorption. Isotherms and BJH pore size distribution are shown in Fig. 5. Sample HS displayed a typical type I isotherm with the characteristic of microporous materials. However, sample AS gave a type III isotherm with a large hysteresis loop starting at $P/P_0 \approx 0.9$, which could be explained by the condensation of nitrogen molecular in pores. The porous space of sample AS was attributed to the interparticle voids with a broad BJH porosity distribution of 5–50 nm, generated by the agglomeration of nanoscale crystalline particles. The textual properties of sample HS and sample AS are listed in Table 1. The micropore surface area and micropore volume of sample HS were 364 m^2/g and 0.17 cm^3/g, respectively, and these values were 359 m^2/g and 0.17 cm^3/g for sample AS. The sample HS and sample AS exhibited very close micropore surface area and micropore volume, which indicated that the crystallinity of the two samples was similar. For sample HS, the BET specific surface area and the external surface area were 425 and 61 m^2/g, respectively, while these values were 550 and 190 m^2/g for sample AS. The rich external surface area of sample AS was consistent with the reduction in particle size observed in the XRD patterns and SEM images.

In order to investigate the content of the organic template in the sample HS and sample AS, the thermogravimetry analysis was carried out and the TG/DSC curves are shown in Fig. 6. One endothermic peak and two exothermic peaks appeared in the DSC curves of both of the two samples. The weight loss with endothermic effect in the temperature range of 100–300 °C were due to the water desorption from zeolites. The sample HS and sample AS contained about 17.9% and 20.7% water before 300 °C, respectively. The weight loss in the temperature range of 300–600 °C of samples HS and AS with exothermic effect were attributed to the removal of organic amine. Notably, the weight loss of organic amine removal from sample AS was more than twice of that from sample HS, which was mainly due to a lot of organic amine adsorbed on the rich external surface area of sample AS being difficult to wash away. The exothermic peaks at high temperature range without weight change of samples HS and AS were attributed to the structural collapse of zeolite framework which could indicate the thermal stability of zeolite ZSM-2. The second exothermic peaks of samples HS and AS appeared in the different temperature range, such as 650–750 °C for the sample HS, while narrower temperature range of about 720–770 °C for sample AS. Detailed weight losses of each stage are listed in Table 2. In general, nanosized ZSM-2 obtained at ambient temperature contained more template agent than micrometer-sized ZSM-2 crystals obtained at high crystallization temperature (100 °C).

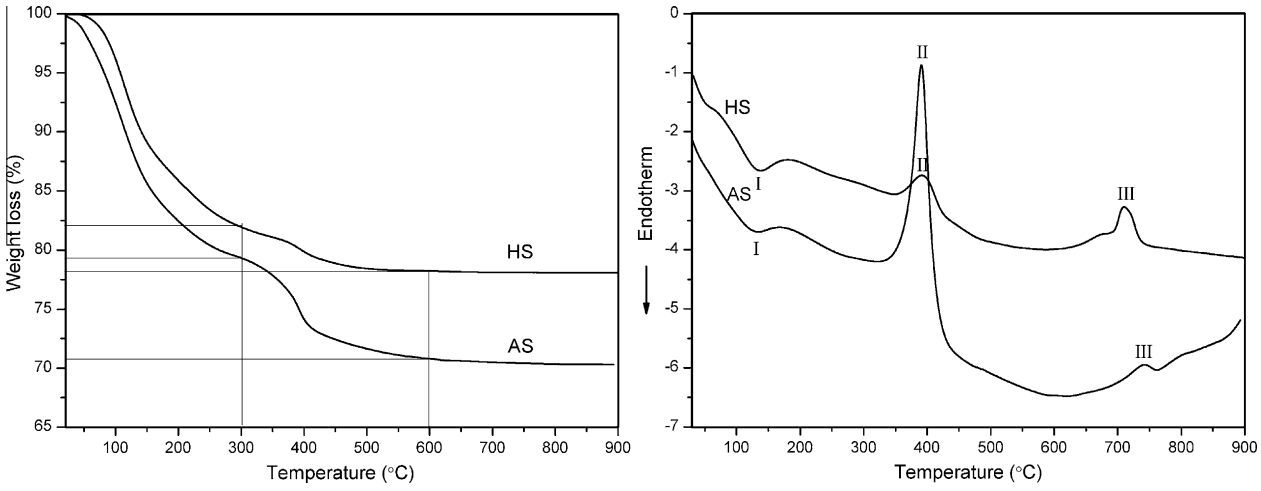

Fig. 6. TG and DSC curves of as-synthesized sample HS and sample AS.

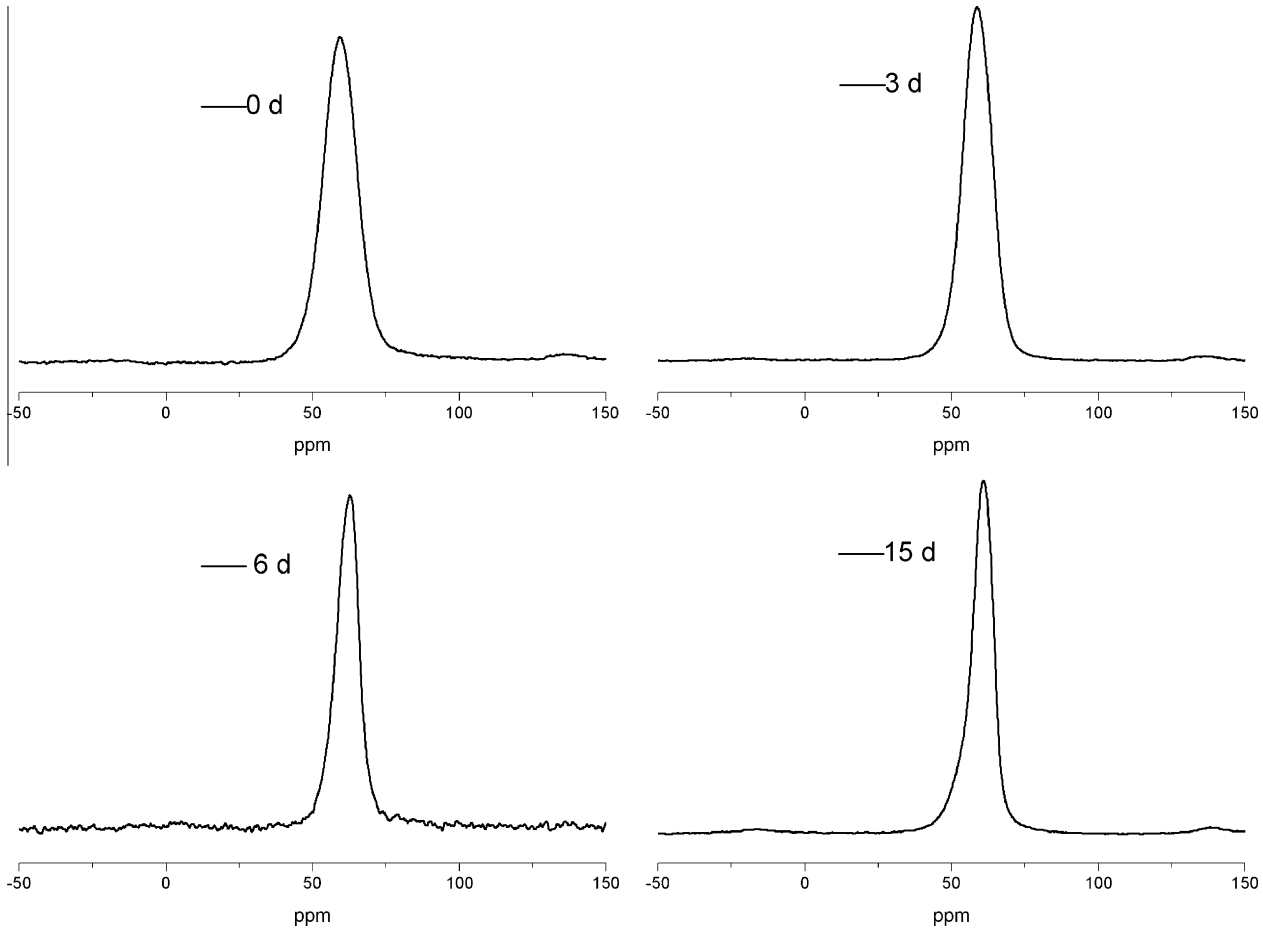

Fig. 7. ^{27}Al NMR spectra for the samples crystallized at ambient temperature for 0, 3, 6, and 15 days.

3.3. NMR study

3.3.1. Investigation of crystallization process

The slow crystallization of ambient synthesis made it possible to study the crystallization process of ZSM-2. In this section, we investigated the transformation of the Al and Si coordination states and textural properties during the ambient crystallization process by means of MAS-NMR and low-temperature N_2 adsorption/desorption analysis.

The ^{27}Al MAS-NMR spectra of the samples obtained after crystallization at ambient temperature for 0, 3, 6, and 15 days are presented in Fig. 7. All of the ^{27}Al MAS-NMR spectra exhibited only a peak centered at about 60 ppm, representative of tetrahedral aluminum species. Furthermore, with prolonging the crystallization time from 0 day to 15 days, the peaks position and peaks width of the ^{27}Al MAS-NMR spectra slightly changed, which was probably due to the aluminum coordination environment becoming uniform and perfect during the crystallization [22].

Fig. 8 demonstrates the ^{29}Si MAS-NMR spectra of the products crystallized at ambient temperature for 0, 3, 6, and 15 days. The sample of 15 d was well crystallized ZSM-2 zeolite as shown in the XRD patterns of Fig. 1. ^{29}Si MAS-NMR spectrum of the sample of 15 d showed a set of split peaks with the chemical shift values range from −110 to −80 ppm, which were assigned to complicated silicon coordination environment in the ZSM-2 zeolite framework [1]. The high resolution of ^{29}Si MAS-NMR spectra had been correlated to the absence of defects in the framework of ZSM-2 sample of 15 d [23]. Other ^{29}Si MAS-NMR spectra of the samples crystallized from 0 day to 6 days also displayed a broad peak with the same chemical shift as the sample after being crystallized for 15 days. Those spectra exhibited slight differences, the spectrum of synthesis gel (0 d) had a small peak at around −112 ppm which was supposed to be amorphous silica in the gel phase and the spectrum of sample 6 d showed split peaks. The ^{27}Al and ^{29}Si MAS-NMR results indicated that the local environment of Al did not change much while that of Si did change a lot during the ambient crystallization process.

The low-temperature N_2 adsorption/desorption analysis of the ZSM-2 samples were performed to investigate the transformation of the micropore area and micropore size distribution during the ambient crystallization process. The N_2 adsorption–desorption isotherms and HK pore size distributions of the samples obtained after 0, 3, 6, and 15 days crystallization are shown in Fig. 9 and the corresponding textual properties are presented in Table 3. As shown in Fig. 9 and Table 3, the samples of 0 d and 3 d displayed small amount of micropore, and the micropore area slightly increased with crystallization time from 0 day to 3 days. The BET specific surface area and *t*-plot micropore area of the sample obtained after 3 days were 157 and 11 m^2/g, respectively. With the increase of crystallization time to 6 days, the BET specific surface area and t-plot micropore area rapidly increased to 302 and 135 m^2/g, respectively. Though the micropores of ZSM-2 after crystallization for 0 day and 3 days were not largely formed, the samples of 0 d and 3 d exhibited obvious micropore size distributions calculated with HK method. The HK pore size distributions of the samples crystallized for 0 day and 3 days displayed a peak at about 0.73 nm, which were similar to that of the ZSM-2 sample crystallized for 15 days with a spike of 0.74 nm. Though the micropore

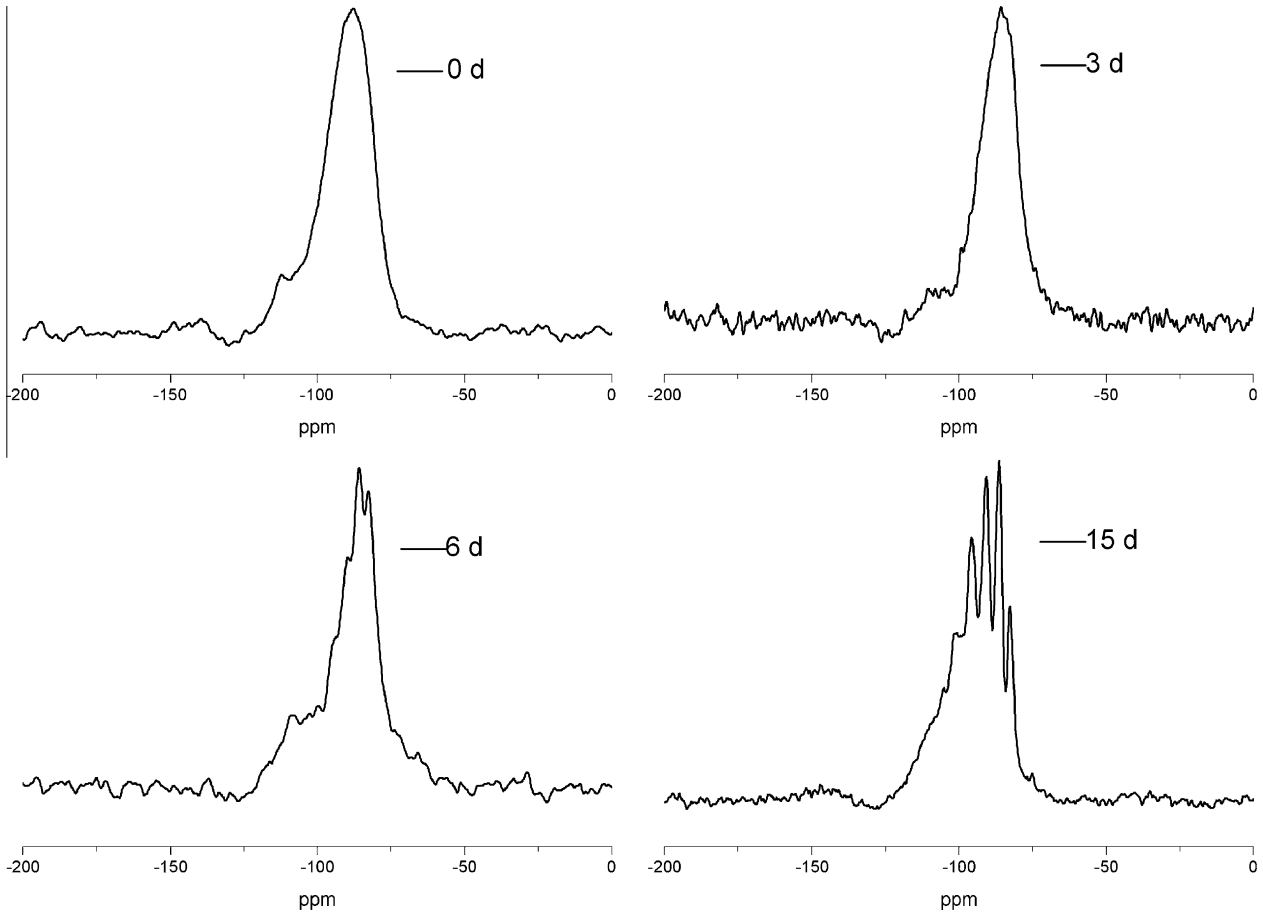

Fig. 8. ^{29}Si NMR spectra for the samples crystallized at ambient temperature for 0, 3, 6, and 15 days.

size distributions of the samples of 0–15 d were similar, the micropores in the samples of 0 d and 3 d might be mainly attributed to aggregation of the particles in the uncrystallized gel mixtures and the micropores in the samples of 6 d and 15 d were mainly ascribed to the FAU and EMT supercage with 12 ring pore opening of around 0.74 nm in diameter.

3.3.2. NMR study for the composition and properties of ZSM-2

^{29}Si MAS-NMR was used to quantify the amount of FAU and EMT phases in ZSM-2 and determine the Si/Al ratio in the two phases individually according to the literature [1]. The ^{29}Si signals of the Na form FAU phase at −102 ppm, −98 ppm, −93 ppm, −88 ppm, and −84 ppm were assigned to Si(0Al), Si(1Al), Si(2Al), Si(3Al) and Si(4Al) species, respectively [24]. The ^{29}Si signals of Li form FAU in the ZSM-2 zeolite systematically upfield shifted by 1 to 2 ppm as compared with the Na form FAU phase [1], and the FAU signals at −101 ppm, −96 ppm, −92 ppm, −87 ppm, and −82 ppm were assigned to Si(0Al)^F, Si(1Al)^F, Si(2Al)^F, Si(3Al)^F and Si(4Al)^F environments in ZSM-2, respectively. However, The signals of the EMT phase in the ZSM-2 zeolite seemed insensitive to the nature of the exchangeable cations [1], which makes the assignment of all Si resonance peaks in Li-ZSM-2 possible. As shown in Fig. 10 and Fig. 11, the signals with no apparent overlapping between FAU and EMT phase at −82 ppm, −99 ppm, −101 ppm, and −105 ppm were assigned to Si(4Al)^F, Si(1Al)^E, Si(0Al)^F and Si(0Al)^E species, respectively. The resonance peak at −86 ppm represented the signal of Si(3Al)^F overlapped by the peak of Si(4Al)^E. The peak centered at −91 ppm was attributed to Si atoms from Si(3Al)^E and Si(2Al)^F chemical environments, and the peak at −96 ppm was assigned to Si atoms from Si(2Al)^E and Si(1Al)^F environments. Using this assignment, the ^{29}Si NMR signals of ZSM-2 were separated into ten individual peaks by Gaussian fitting method, and then the FAU and EMT phases could be discriminated, respectively. As shown in Table 4, sample HS crystallized at 100 °C contained 59% FAU and 41% EMT phase, with a Si/Al ratio of 1.86 and 1.95, respectively. However, Sample AS, crystallized at ambient temperature, contained 53% FAU phase with a Si/Al ratio of 1.42 and 47% EMT phase with a Si/A1 ratio of 1.48. These results suggested that sample AS obtained by ambient synthesis contained 6% more EMT phase as compared with sample HS performed at 100 °C. The result was similar to the literature [17], Eng-Poh Ng et al. found the EMT was the first kinetic, metastable product under ambient temperature, followed by its conversion to the more stable cubic FAU and more dense SOD structures. In addition, the Si/Al ratio of sample AS obtained by ambient synthesis was more lower than the Si/Al ratio of sample HS performed at 100 °C, which was consistent with lattice energy minimization calculations [25]. The lattice energy was enhanced with the increase the Si/Al ratio of FAU, so it required higher temperature to crystallize. Furthermore, the FAU phase and EMT phase in the same sample exhibited different Si/Al ratio, the EMT phase possessed higher Si/Al ratio than the FAU phase. In conclusion, the nanoscale ZSM-2 obtained by ambient synthesis contained more EMT phase and lower Si/Al ratio than micrometer-sized ZSM-2 crystals obtained at 100 °C.

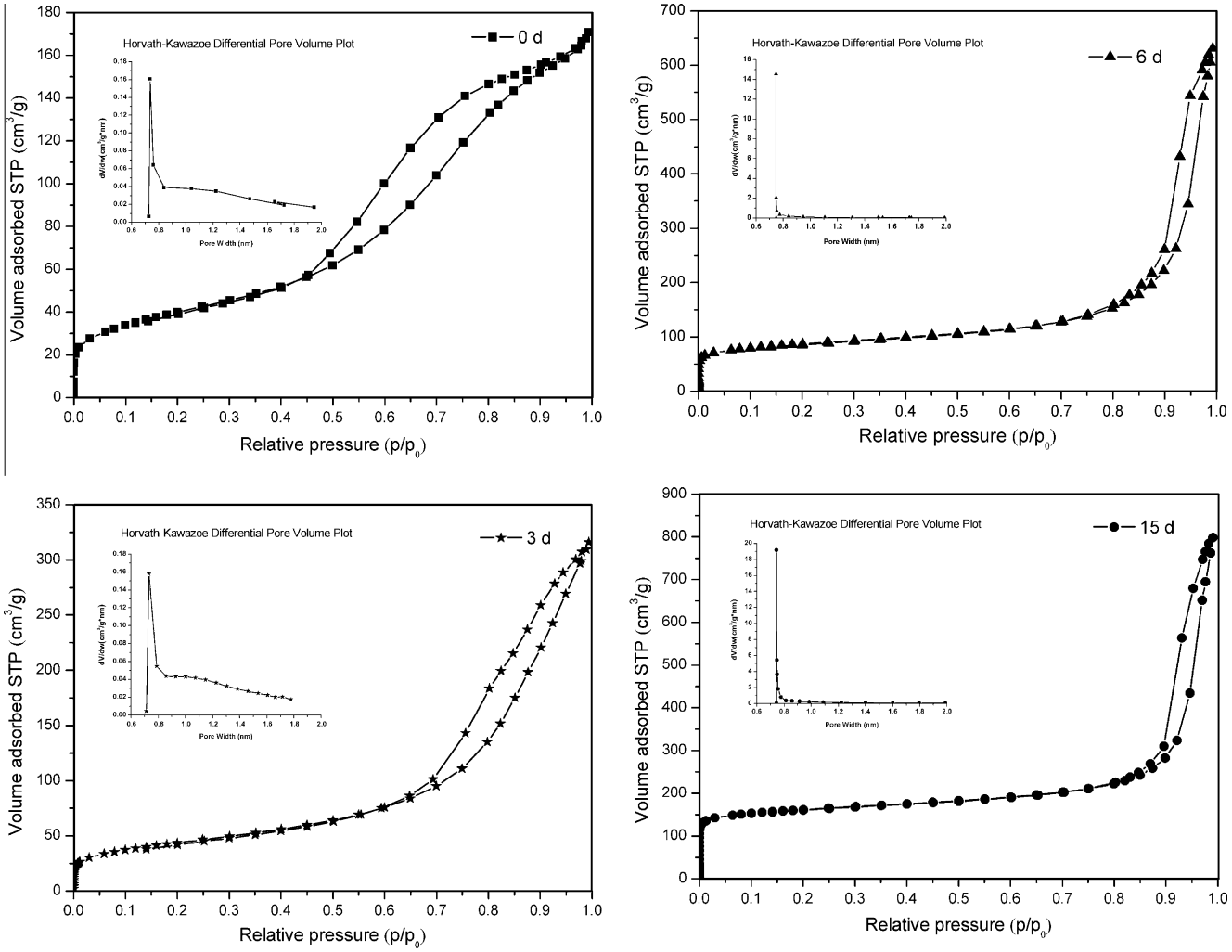

Fig. 9. N_2 adsorption–desorption isotherms and HK porosity distribution of samples crystallized at ambient temperature for 0, 3, 6, and 15 days.

Table 3
Textual properties of the samples crystallized at ambient temperature for 0, 3, 6, and 15 days.

Sample	Surface area (m^2/g)			Pore volume (cm^3/g)	
	S_{total} [a]	S_{micro} [b]	S_{ext} [c]	V_{total}	V_{micro} [d]
0 d	143	7.66	136	0.252	0.00189
3 d	157	11.6	146	0.459	0.00367
6 d	302	135	166	0.838	0.0621
15 d	550	359	190	1.007	0.166

[a] BET surface area.
[b] *t*-plot micropore surface area.
[c] *t*-plot external surface area.
[d] *t*-plot micropore volume.

4. Conclusions

In this work, ZSM-2 nanorods with crystal size about 50 nm have been successfully synthesized at ambient temperature. According to ambient crystallization kinetic curve and XRD characterizations, the crystallization process of ZSM-2 zeolite under ambient temperature included the inducing period, rapid growth period and stable crystallinity period. Furthermore, the samples performed at ambient temperature (30 °C) and high temperature (100 °C) showed different characteristics. The sample obtained at

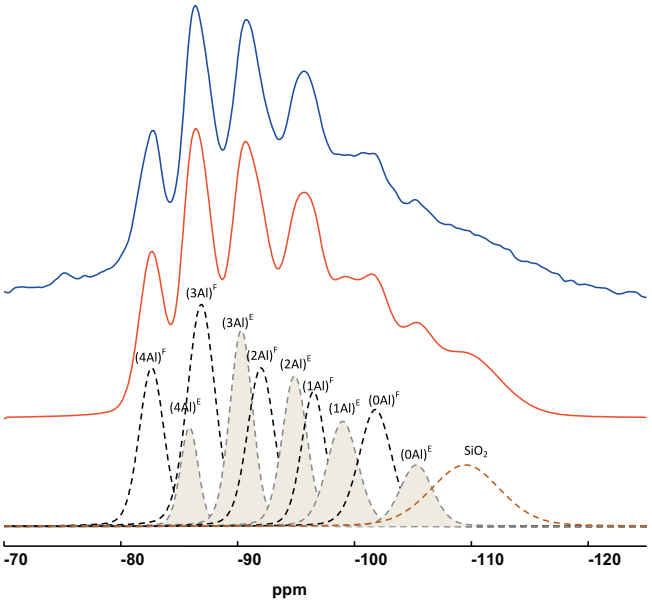

Fig. 10. ^{29}Si MAS-NMR spectra of as-synthesized sample HS.

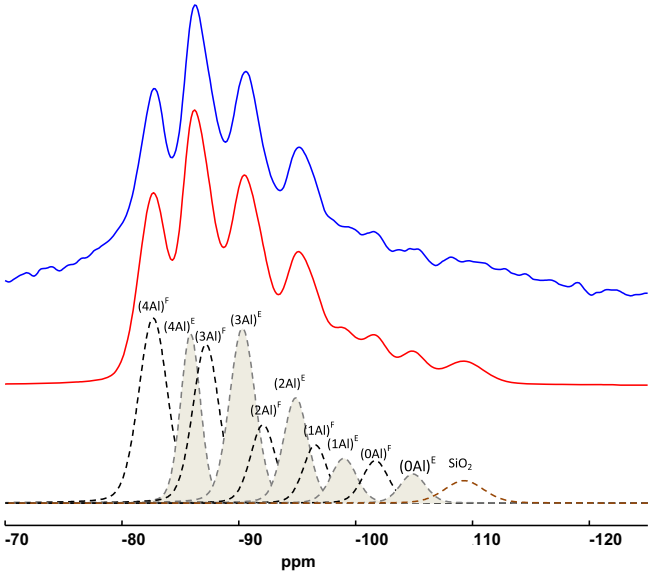

Fig. 11. ^{29}Si MAS-NMR spectra of as-synthesized sample AS.

Table 4
Phase composition and Si/Al ratio in the FAU and EMT domains of sample HS and sample AS determined by ^{29}Si MAS-NMR.

Sample	Si/Al atomic ratio		
	FAU phase	EMT phase	Overall
HS	1.86	1.95	1.90
AS	1.42	1.48	1.45
	$(Si + Al)^F/(Si + Al)^{E+F}$ (%)	$(Si + Al)^E/(Si + Al)^{E+F}$ (%)	
HS	59	41	
AS	53	47	

100 °C displayed two different morphologies of micron-sized ZSM-2, while the sample obtained by ambient synthesis exhibited rod-like crystals of ZSM-2 with the crystal size of 50 nm around. The XRD peaks of ZSM-2 synthesized at ambient temperature significantly broaden due to their nanosize of the crystals. Physical adsorption and thermal analysis proved that ZSM-2 zeolite synthesized at ambient temperature possessed large external surface area and total pore volume and contained relatively large amount of organic template as compared with the sample synthesized at 100 °C. More EMT phase and lower Si/Al ratio presented in nanoscale ZSM-2 obtained by ambient synthesis. Further investigation into the crystallization process of ambient synthesis by means of NMR and low-temperature N_2 adsorption/desorption characterizations indicated that the local environment of Al did not change much while that of Si did change a lot during the ambient crystallization process, and the micropore area increased rapidly with increasing crystallization time while the micropore size distributions of the samples of 0–15 d were similar.

Since the ZSM-2 nanocrystals synthesized under ambient temperature possess small zeolite crystals and large external surface areas, the samples will expose more active centers and lower mass and heat transfer resistance than micron-sized ZSM-2 zeolite in catalytic reactions, so they are expected to exhibit good catalytic activity in many reactions catalyzed by EMT/FAU type zeolite, such as FCC process.

References

[1] J.A. Martens, Y.L. Xiong, E.J.P. Feijen, P.J. Grobet, P.A. Jacobs, J. Phys. Chem. 97 (1993) 5132–5135.
[2] C. Covarrubias, R. Quijada, R. Rojas, Microporous Mesoporous Mater. 117 (2009) 118–125.
[3] J. Ciric, U.S. Patent 3411,874, 1968.
[4] R.M. Barrer, W. Sieber, J. Chem. Soc. Dalton Trans. (1977) 1020.
[5] B.J. Schoeman, J. Sterte, J.E. Otterstedt, J. Colloid Interface Sci. 170 (1995) 449–456.
[6] L. Tosheva, V.P. Valtchev, Chem. Mater. 17 (2005) 2494–2513.
[7] B.J. Schoeman, J. Sterte, J.E. Otterstedt, Zeolites 14 (1994) 110–116.
[8] S. Mintova, V. Valtchev, Studies in Surface Science and Catalysis, Elsevier, 1999 (pp. 141–148).
[9] S. Mintova, N.H. Olson, T. Bein, Angew. Chem. Int. Ed. 38 (1999) 3201–3204.
[10] S. Mintova, N.H. Olson, V. Valtchev, T. Bein, Science 283 (1999) 958–960.
[11] Q. Li, D. Creaser, J. Sterte, Chem. Mater. 14 (2002) 1319–1324.
[12] C. Madsen, C.J.H. Jacobsen, Chem. Commun. (1999) 673–674.
[13] I. Schmidt, C. Madsen, C.J.H. Jacobsen, Inorg. Chem. 39 (2000) 2279–2283.
[14] C.J.H. Jacobsen, C. Madsen, T.V.W. Janssens, H.J. Jakobsen, J. Skibsted, Microporous Mesoporous Mater. 39 (2000) 393–401.
[15] L.B. Sand, A. Sacco, R.W. Thompson, A.G. Dixon, Zeolites 7 (1987) 387–392.
[16] V.P. Valtchev, K.N. Bozhilov, J. Phys. Chem. B 108 (2004) 15587–15598.
[17] E.P. Ng, D. Chateigner, T. Bein, V. Valtchev, S. Mintova, Science 335 (2011) 70–73.
[18] C.J.J. Denouden, R.W. Thompson, Ind. Eng. Chem. Res. 31 (1992) 369–373.
[19] K. Chung, K. Kim, G. Seo, Korean J. Chem. Eng. 9 (1992) 144–149.
[20] A.W. Burton, K. Ong, T. Rea, I.Y. Chan, Microporous Mesoporous Mater. 117 (2009) 75–90.
[21] E.P. Ng, J.M. Goupil, A. Vicente, C. Fernandez, R. Retoux, V. Valtchev, S. Mintova, Chem. Mater. 24 (2012) 4758–4765.
[22] L. Gora, K. Streletzky, R.W. Thompson, G.D.J. Phillies, Zeolites 18 (1997) 119–131.
[23] C.A. Fyfe, H. Gies, G.T. Kokotailo, C. Pasztor, H. Strobl, D.E. Cox, J. Am. Chem. Soc. 111 (1989) 2470–2474.
[24] M. Ogura, Y. Kawazu, H. Takahashi, T. Okubo, Chem. Mater. 15 (2003) 2661–2667.
[25] I. Petrovic, A. Navrotsky, Microporous Mater. 9 (1997) 1–12.